Applied Physics A (2022) 128:470
https://doi.org/10.1007/s00339-022-05620-y

Applied Physics A
Materials Science & Processing

The significant role of WO_3 on high-dense $BaO–P_2O_3$ glasses: transmission factors and a comparative investigation using commercial and other types of shields

H. O. Tekin[1,2] · Ghada ALMisned[3] · Y. S. Rammah[4] · G. Susoy[5] · Fatema T. Ali[6] · Duygu Sen Baykal[7] · W. Elshami[1] · Hesham M. H. Zakaly[8,10] · Shams A. M. Issa[9,10]

Received: 14 April 2022 / Accepted: 19 April 2022

Abstract

The direct effects of tungsten trioxide (WO_3) on gamma radiation attenuation properties of tungsten/barium/phosphate glasses with chemical form xWO_3–(50-x/2)BaO–(50-x/2)P_2O_3, x = 0 (S1)–60 (S7) in steps of 10 mol% has been investigated. To this end, Phy-X/PSD software and Monte Carlo code were applied. The increased amount of WO_3 in the glass composition, on the other hand, contributed positively to the increase in density and radiation sensing properties. At the lowest and highest WO_3 contributions, a nearly twofold increase in HVL value was seen for the S1 and S7 glass samples, respectively, with S7 having the lowest HVL values. The HVL has obeyed the trend as: $(HVL)_{S1} > (HVL)_{S2} > (HVL)_{S3} > (HVL)_{S4} > (HVL)_{S5} > (HVL)_{S6} > (HVL)_{S7}$. The variation of the tenth value layer (TVL) for all studied glasses has the same trend of HVL. In terms of mean free path (MFP), there was negative effect of WO_3 concentration on the trend of MFP. Consequently, S7 glass sample has the lowest values of MFP, while the S1 glass sample has the highest values. Therefore, $(MFP)_{S1} > (MFP)_{S2} > (MFP)_{S3} > (MFP)_{S4} > (MFP)_{S5} > (MFP)_{S6} > (MFP)_{S7}$. A comparison of the HVL of S7 glass sample with some commercial radiation shielding materials such as different types of concrete and RS-253-G18 glasses has been performed and concluded that the S7 glass sample is superior as radiation shielding material than several commercial materials. It can be concluded that WO_3 reinforcement serves a multipurpose of increasing the density and hence the gamma-ray-shielding characteristics of comparable glass compositions.

Keywords $BaO–WO_3–P_2O_5$ glass system · Elastic moduli · Radiation shielding · MCNPX

✉ H. O. Tekin
tekin765@gmail.com

✉ Ghada ALMisned
gaalmisned@pnu.edu.sa

[1] Department of Medical Diagnostic Imaging, College of Health Sciences, University of Sharjah, 27272 Sharjah, United Arab Emirates

[2] Faculty of Engineering and Natural Sciences, Computer Engineering Department, Istinye University, 34396 Istanbul, Turkey

[3] Department of Physics, College of Science, Princess Nourah Bint Abdulrahman University, P.O. Box 84428, Riyadh 11671, Saudi Arabia

[4] Department of Physics, Faculty of Science, Menoufia University, Shebin El-Koom 32511, Menoufia, Egypt

[5] Department of Physics, Faculty of Science, Istanbul University, 34134 Istanbul, Turkey

[6] Center for Advanced Materials Research, Research Institute of Sciences and Engineering, University of Sharjah, 27272 Sharjah, United Arab Emirates

[7] Vocational School of Health Sciences, Medical Imaging Techniques, Istanbul Kent University, 34433 Istanbul, Turkey

[8] Institute of Physics and Technology, Ural Federal University, 620002 Ekaterinburg, Russia

[9] Physics Department, Faculty of Science, University of Tabuk, Tabuk 47512, Saudi Arabia

[10] Physics Department, Faculty of Science, Al-Azhar University, Assiut 71524, Egypt

Published online: 07 May 2022

1 Introduction

Lead (Pb) and Pb-based materials are the most utilized materials in radiation protection applications. Recent investigations, however, have revealed that the hazardous consequences of Pb on people's health and the environment, in general, are severe problems due to its toxicity. Consequently, its use as a shielding material is restricted. Following Pb, concrete is yet another material that is well suited for shielding of ionizing electromagnetic radiation types such as gamma-ray and X-ray. Nevertheless, its primary disadvantage is that it is largely used in the building of shields and is very heavy and costly. Concrete, on the other hand, tends to crack when it is used. Alternative materials in radiation protection studies are alloys, rocks, marbles, slag, precious stones, steel, polymers, lead-based materials, and lead-free materials [1, 2]. On the other hand, glass is an efficient radiation shielding material for gamma-rays due to its transparency to visible light, simplicity of manufacture, high amount of recyclability, and ease of property modification through preparation and composition operations [3–6]. To improve the shielding properties, a variety of radiation-shielding glasses have been produced considering their optical, mechanical, structural, and other related properties [7, 8]. Meanwhile, Phosphate (P) glasses have distinct features that allow them to be used in a variety of applications. Different varieties of these glasses could be useful in a variety of fields. Phosphorus oxide-based glasses have been investigated as attractive materials for a variety of applications in recent years due to their low viscosity, low melting and glass transition temperatures, high refractive indices, and great thermal expansion. The employment including both network formers and glass modifiers may help enhance the phosphate glasses' poor chemical durability [9–14]. However, by including appropriate oxides within the glass structure, the characteristics of phosphate glasses may be increased. Glasses containing elements with a high Z number (elements having a big atomic number but a small gamma-ray cross-section), such as Ba (Z = 56), W (Z = 74), Pb (Z = 82), and Bi (Z = 83), are some great choices for shielding people from X-ray, gamma-ray, and neutron interference radiation. A balanced mix of low and high Z elements is required for shielding materials against gamma and neutron combinations [15]. Tungsten trioxide (WO_3) is one of the few oxides that may form glasses with P2O5 over a wide range of compositions [16, 17]. The doping level of tungsten trioxide glasses is extremely dependent on the glass forming process; however, they are exciting technical materials. An intriguing optical feature of tungsten trioxide is used in solid-state micro batteries, optical smart windows, display devices and gas sensors [18–21]. For several purposes, glasses incorporating WO_3 have been developed. There are a variety of applications for amorphous semiconductors that include smart windows, anti-glare rear view mirrors, optical recording devices and non-emitting displays [22–26]. There are also sensors for temperature and humidity, solid-state gas sensors, biosensors, and mechanical and thermal sensors [23–26]. To compensate for the loss of bridging oxygens caused by the alkaline earth oxides (CaO, SrO, and BaO) added to P_2O_5, non-bridging oxygens are produced instead. Barium oxide glasses, rather than lead or zinc oxide glasses, have two advantages: the first is that they are lead-free, and the second is that they are more chemically, thermally, and mechanically resistant than zinc phosphate glasses. With the addition of BaO to phosphate-based glasses, the optical band gap energy increases while the refractive index decreases slightly. According to the literature, BaO can be employed as a suitable radiation shielding material in a variety of glass matrices with good optical properties [27, 28]. Radiation shielding properties of glass include its ability to absorb gamma-rays and neutrons, as well as its transparency and the ability to simply modify its composition. Since glass systems have such different properties, they've attracted the interest of many radiation shielding researchers. Analysis of mass attenuation coefficients (MAC), half values, tenth values, mean free path, Z_{eff} effective number, exposure build-up factor, energy absorption build-up factor were all calculated in this study (EABF). MCNPX general purpose Monte Carlo simulation code [29] and Phy-X/PSD [30] program was used to determine the transmission factor (TF), and other essential gamma-ray-shielding parameters. The obtained results were also compared with some conventional and commercial shielding materials in a wide energy range. The findings of this research may be useful for evaluating the materials created in the source article on a large scale, as well as for gaining a better knowledge of the absorption enhancement offered by the WO_3 addition in relation to the percentage increase in the glass compositions investigated.

2 Materials and methods

2.1 Bismuth borosilicate glasses

To achieve the aims of this study, seven glass samples of tungsten/barium/phosphate glasses with chemical formula xWO_3–(50-x/2)BaO–(50-x/2)P_2O_3, x = 0–60 in steps of 10 mol% were chosen from the previous work [31]. In a previous study on this group of materials, Sayyed et al. [32] explored gamma-ray reduction characteristics for a particular and limited energy range. Going beyond this research, in this study, the gamma-ray energies of nuclear type radioisotopes

are utilized to determine TF factors, which will give important information for more practical applications by maintaining the photon energy range explored in this study considerably larger. A few more essential shielding metrics like as build-up factors that were not offered in the prior research were also given in this study, thereby broadening the size of the current study. Detailed information of the investigated glasses is stated as follows:

S1: $0WO_3–50BaO–50P_2O_5$: density (ρ = 3.64 g/cm^3 and molar volume (V_m = 40.6 cm^3/mol)),

S2: $10WO_3–45BaO–45P_2O_5$: density (ρ = 3.89 g/cm^3 and molar volume (V_m = 40.1 cm^3/mol)),

S3: $20WO_3–40BaO–40P_2O_5$: density (ρ = 4.18 g/cm^3 and molar volume (V_m = 39.4 cm^3/mol)),

S4: $30WO_3$-$35BaO–35P_2O_5$: density (ρ = 4.48 g/cm^3 and molar volume (V_m = 38.6 cm^3/mol)),

S5: $40WO_3–30BaO–30P_2O_5$: density (ρ = 4.88 g/cm^3 and molar volume (V_m = 37.4 cm^3/mol)),

S6: $50WO_3–25BaO–25P_2O_5$: density (ρ = 5.16 g/cm^3 and molar volume (V_m = 36.8 cm^3/mol)), and.

S7: $60WO_3–20BaO–20P_2O_5$: density (ρ = 5.47 g/cm^3 and molar volume (V_m = 36.2 cm^3/mol)).

All details and elemental weight fraction of the studied glasses are collected in Table 1.

2.2 Calculation of transmission factors (TFs) using MCNPX code

Another critical characteristic of radiation shielding materials is their ability to absorb a fraction of the primary radiation impacting on attenuator. This condition may be represented in terms of the value produced from the proportionate assessment of the primary–secondary radiation beam pair used to determine the entire material, rather than the explicitly stated gamma-ray-shielding parameters. The physical equivalent of this application is the shielding material's transmission factor (TF) [33]. The TF values of the glass samples tested in this research were carefully explored for a variety of radioisotopes used therapeutically and diagnostically in the nuclear type (see Table 2). For this portion of the investigation, the MCNPX algorithm is used to simulate a wide transmission assembly. Figure 1 shows a three-dimensional depiction of the setup built using the MCNPX algorithm. As shown in the figure, the quantity of gamma rays' incident on and absorbed by the glass material in the center of the two detection zones were the primary parameters utilized to calculate the TF values. In addition, to determine the fluctuation in TF values with thickness, each glass sample was modeled in various thicknesses and the radioisotopes given in Table 2 were determined. The infrastructure for the modeling shown in Fig. 1 began with the development of the MCNPX INPUT file and concluded with the export of the TALLY values from the OUTPUT file and the definition of the TF values. Additional technical details on TF simulation may be gleaned from our prior research and the literature [34, 35].

Table 2 Radioisotopes and gamma-ray energies used for gamma-ray TF calculations

Radioisotope	Gamma-ray energy (MeV)
^{67}Ga	0.0086, 0.0093, 0.1840
^{57}Co	0.0144, 0.1221, 0.1365
^{111}In	0.0230, 0.1710, 0.2450
^{133}Ba	0.0532, 0.0796, 0.0810, 0.2764, 0.3029, 0.3560, 0.3838
^{201}Tl	0.0710, 0.1350, 0.1670
^{99m}Tc	0.1405
^{51}Cr	0.3201
^{131}I	0.2843, 0.3645, 0.6370, 0.7229
^{58}Co	0.5110, 0.8108
^{137}Cs	0.6617
^{60}Co	1.1732, 1.3325

Table 1 Samples code, elemental weight fraction, density, and molar volume of (50-x/2)BaO–xWO_3–(50-x/2)P_2O_3: (x = 0,10, 20, 30, 40, 50, and 60 mol% glasses

Samples code	Elemental weight fraction (wt.%)				Density, ρ (g/cm^3) [30]	Molar volume, V_m (cm^3/mol) [30]
	O	*P*	Ba	W		
S1	0.325104	0.2098	0.465097	0	3.64	40.6
S2	0.307562	0.178632	0.396002	0.117804	3.89	40.1
S3	0.291817	0.150655	0.333981	0.223546	4.18	39.4
S4	0.277606	0.125403	0.278002	0.318989	4.48	38.6
S5	0.264714	0.102497	0.227222	0.405567	4.88	37.4
S6	0.252967	0.081624	0.180948	0.484461	5.16	36.8
S7	0.242218	0.062524	0.138608	0.556651	5.47	36.2

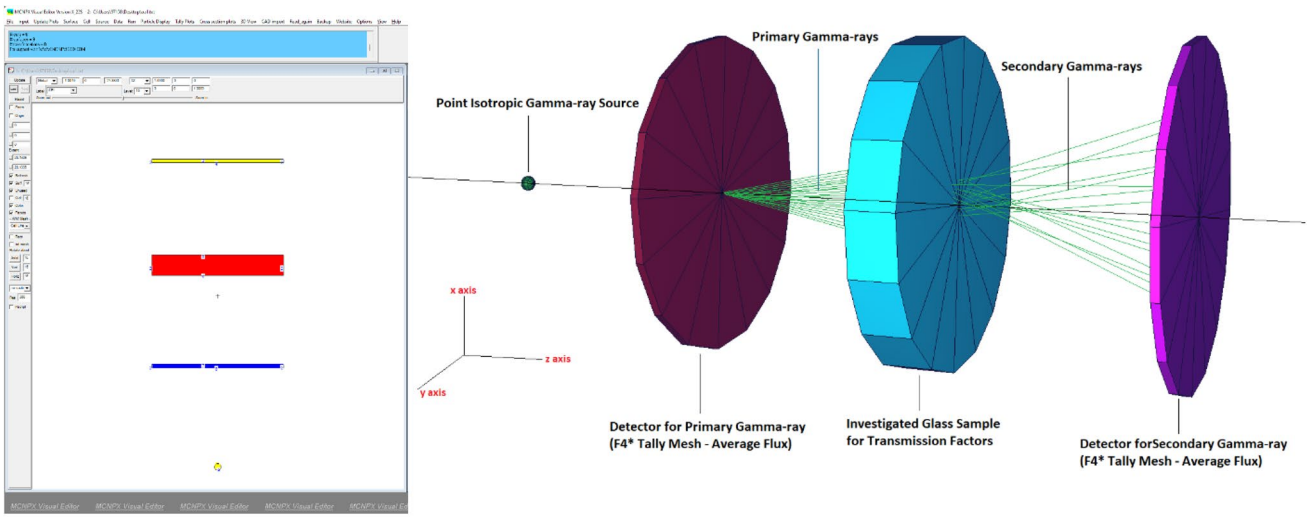

Fig. 1 **(a)** 2-D view of designed MCNPX simulation setup **(b)** 3-D illustration of designed MCNPX setup (2-D and 3-D views are obtained from MCNPX Visual Editor VisedX22S)

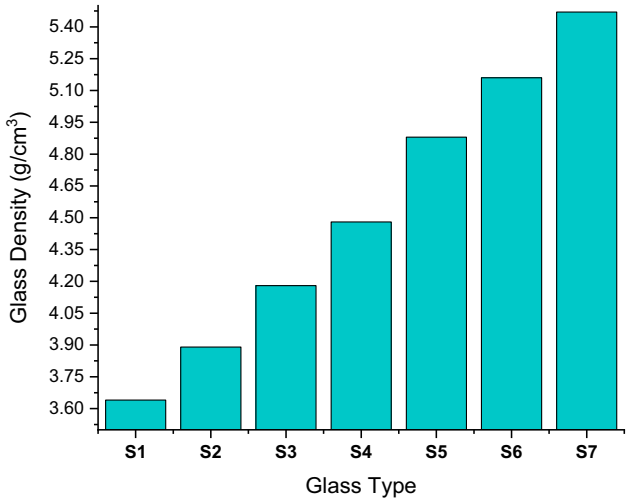

Fig. 2 Variation of investigated glass densities

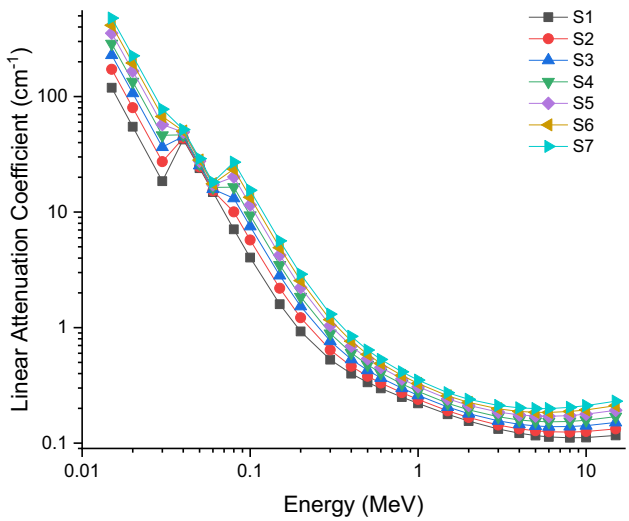

Fig. 3 Variations of linear attenuation coefficient (cm^{-1}) with photon energy (MeV) for all S1–S7 glasses

3 Results and discussion

The radiation attenuation characteristics of seven distinct glass samples doped with varying quantities of WO_3 were studied in this work. The WO_3 additive ratio was gradually raised in several glass compositions from S1 to S7 and achieved its highest value in the S7 sample. Figure 2 illustrates the variation in density of the studied glass samples as the quantity of WO_3 in the glass composition increases. This increase in weight resulted in a rise in the elements composition and a considerable increase in glass density, resulting in a difference of 1.83 g/cm^3 between the lowest and maximum WO_3 reinforcement. Among the gamma-ray-shielding properties, the linear attenuation coefficient (μ) is the one that is proportional to the material density. A material's linear attenuation coefficient is a crucial parameter that can be computed for each gamma-ray energy and serves as the fundamental condition for calculating other critical parameters. Figure 3 illustrates the pattern of change in linear attenuation coefficients determined for seven different glass samples as a function of gamma-ray. As seen in the image, the linear attenuation

coefficient values are presented as maximal in the low energy zone. This is because the photoelectric effect is the main mechanism for low energy photons. This large reduction in the low energy area created a peak for the k-absorption edge and then declined again, indicating that Compton scattering was the dominating interaction in the mid-level energy region and that the decrease was accompanied by a lighter acceleration. As seen in Fig. 3, the elemental compositions of the seven glass samples investigated had a substantial effect on the linear attenuation coefficient values. As a consequence, S7 samples with the highest rate of WO_3 addition had the highest linear attenuation coefficients for all energy values investigated. This demonstrates that the increase in density caused by doping also has a major influence on the linear attenuation coefficient in multi-glass samples. The half value layer (HVL) is another critical gamma-ray-shielding characteristic that can be calculated using the linear attenuation coefficient. The HVL physically represents the thickness at which the amount of a photon of a certain energy incident on a material will reduce to half its value. The fact that this thickness varies for the same energy values indicates that materials with a low half value thickness have better gamma-ray attenuation characteristics. In other words, decreasing a material's HVL value for a given photon energy improves its shielding properties. Figure 4 illustrates the range in HVL values between 0.015 and 15 MeV energy for the seven different glass samples investigated. As seen in the figure, although the HVL values are modest for low photon energies, a proportionate increasing trend in the HVL values has begun as photon energy increases. The primary explanation for this condition is that the higher WO_3 additive ratio results in a rise in the linear attenuation coefficients, which results in a fall in the HVL values (i.e., $HVL = 0.693/\mu$). As a consequence, the S7 sample received the lowest HVL values. A deeper analysis of Fig. 4 reveals an average difference of two times between S1 and S7 samples for the same energy value, particularly in the high energy range. This is another situation where the WO_3 addition noticeably improves shielding for the two samples with the lowest and highest doping percentages. Generally, HVL has followed the trend as: $(HVL)_{S1} > (HVL)_{S2} > (HVL)_{S3} > (HVL)_{S4} > (HVL)_{S5} > (HVL)_{S6} > (HVL)_{S7}$. Figure 5 shows the variation of the tenth value layer ($TVL = 2.302/\mu$) as a function of photon energy in MeV for all studied glasses. From Fig. 5, it was observed that TVL parameter has a similar trend of HVL for all studied glasses. In terms of mean free path ($MFP = 1/\mu$), the variations of MFP with the incident photon (E) for S1–S7

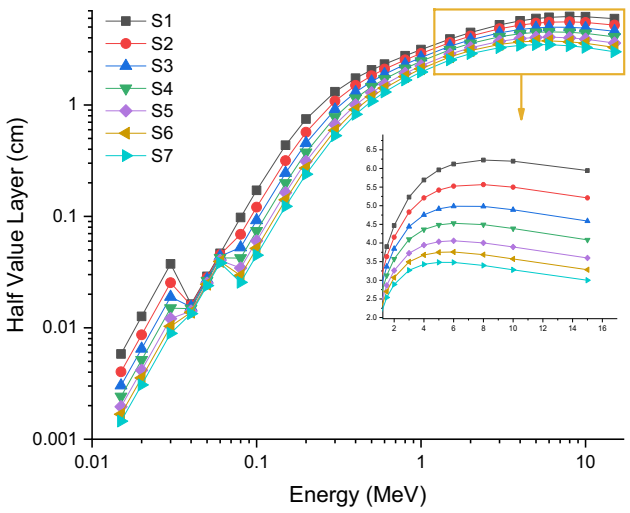

Fig. 4 Variations of half value layer (cm) with photon energy (MeV) for all S1–S7 glasses

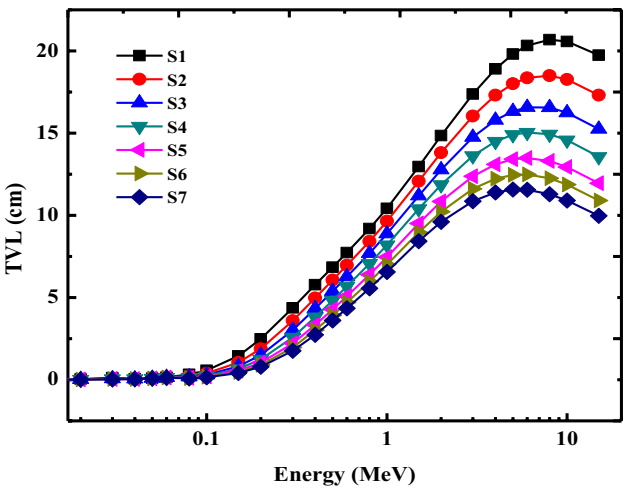

Fig. 5 Variations of tenth value layer (cm) with photon energy (MeV) for all S1–S7 glasses

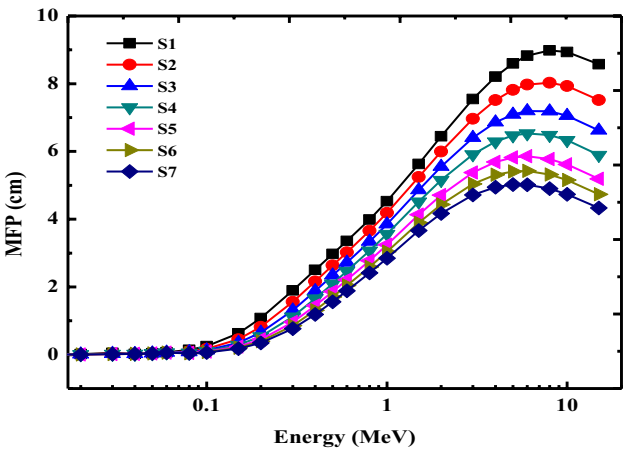

Fig. 6 Variations of mean free path (cm) with photon energy (MeV) for all S1–S7 glasses

glasses is depicted in Fig. 6. As shown in this figure, there was negative effect of WO_3 concentration on the trend of MFP. Consequently, S7 glass sample has the lowest values of MFP = 0.002 cm at photon energy 15 keV and 4.329 cm at photon energy 15 MeV, while the S1 glass sample has the highest values of MFP = 0.008 cm and 8.584 cm at photon energy 0.015 MeV and 15 MeV, respectively. Therefore, $(MFP)_{S1} > (MFP)_{S2} > (MFP)_{S3} > (MFP)_{S4} > (MFP)_{S5} > (MFP)_{S6} > (MFP)_{S7}$. Results of the HVL, TVL, and MFP confirm that the S7 glasses have the best shielding capacity among all investigated glasses. Figure 7 shows a comparison of the HVL of S7 glass sample with some commercial radiation shielding materials such as Ordinary concrete (OC) [36], Hematite–Serpentine concrete (HSC), (Ilmenite–Limonite concrete (ILC), Basalt–Magnetite concrete (BMC), Ilmenite concrete (IC), Steel-Scrap concrete (SSC), Steel–magnetite (SMC) [36], and RS-253-G18 glasses [37]. From Fig. 7, it was observed that the S7 glass sample is superior as radiation shielding material than several commercial materials. Figure 8 illustrates the variation of the effective atomic number (Z_{eff}) with photon energy (MeV) for all S1-S7 glasses. The maximum Z_{eff} values were recorded in this energy zone due to the prevalence of photoelectric contact. As a result of the increase in Z (W = 74) in the glass matrix, a statistically significant rise in Z_{eff} was seen in the lowest energy band. As a result, the Z_{eff} values in the intermediate energy zone reduced dramatically as a result of the frequency of Compton scattering occurring in the intermediate energy region. According to our results, the S7 sample with the greatest mass attenuation coefficients also has the maximum feasible Z_{eff} values at the energies under consideration. Variances in exposure build-up factor (EBF) and energy

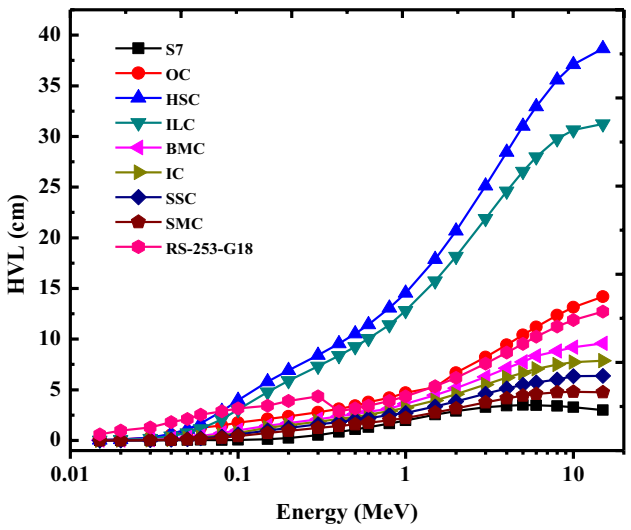

Fig. 7 Comparison between HVL of sample S7 with some commercial materials in photon energy (MeV)

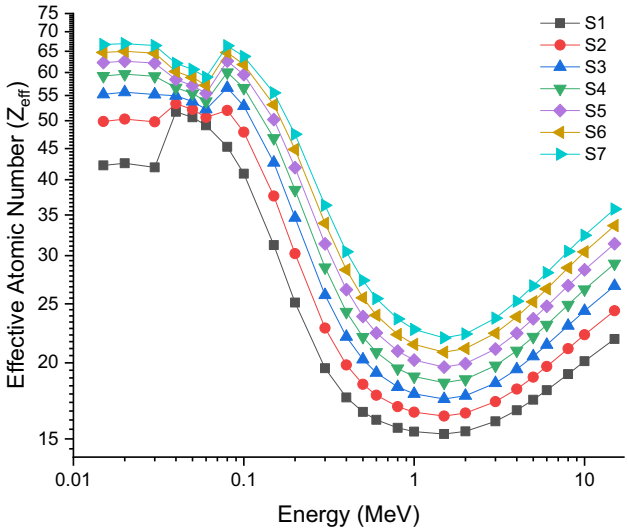

Fig. 8 Variations of effective atomic number (Z_{eff}) with photon energy (MeV) for all S1–S7 glasses

absorption build-up factor (EABF) values are shown in Figs. 9 and 10 as a function of gamma-ray energy (MeV) over a range of mean free path values. Since photoelectric absorption accounts for the vast majority of incoming gamma-rays in the low gamma-ray energy area, as can be shown, both EBF and EABF values are very low in the low gamma-ray energy range. The EBF and EABF values, on the other hand, dramatically increase when Compton Scattering becomes evident around roughly 0.1 MeV. According to our results, increasing the amount of WO3 supplementation resulted in a decrease in the EBF and EABF values across the board (i.e., from 0.5 to 40 mfp). In other words, when the amount of W grows from S1 to S7, the collision rate of incoming gamma-rays increases considerably in the glass samples. Figure 1 shows the effect of increasing the quantity of W. Finally, another crucial parameter for shielding materials, the gamma-ray transmission factor (TF), was calculated for S1, S2, S3, S4 and S5 glass samples for a range of well-known radioisotope energies (see Table 2). The TF values of the investigated glasses were determined using two distinct methods. To begin, the TF factors of S1–S7 samples were determined at varied glass thicknesses. At different glass thicknesses, in Fig. 11, the TFs of the studied glasses are shown as a function of the radioisotope energy (MeV). The transmission factor rises in synch with the radioisotope energy, from 0.0086 MeV to 1.3326 MeV. When testing at low energies, the lowest TF values were found in glass samples of all thicknesses tested. Low-energy gamma-rays may be easily attenuated by thick samples because of their high attenuation capacity Thus, at around 0.1 MeV, there is a significant discrepancy. As the gamma-ray energy

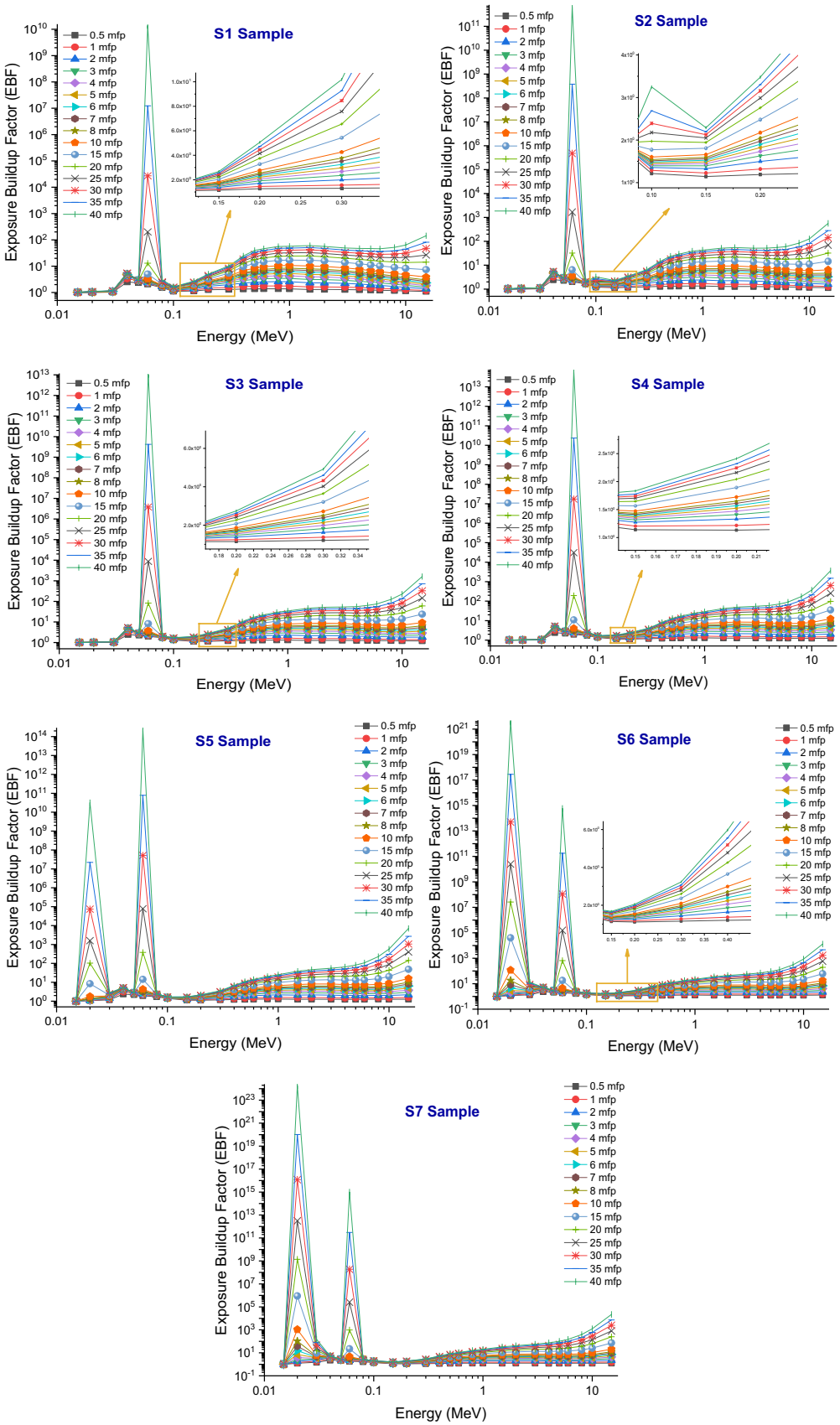

Fig. 9 Variation of EBF values as a function of photon energy at 0.5–40 mfp

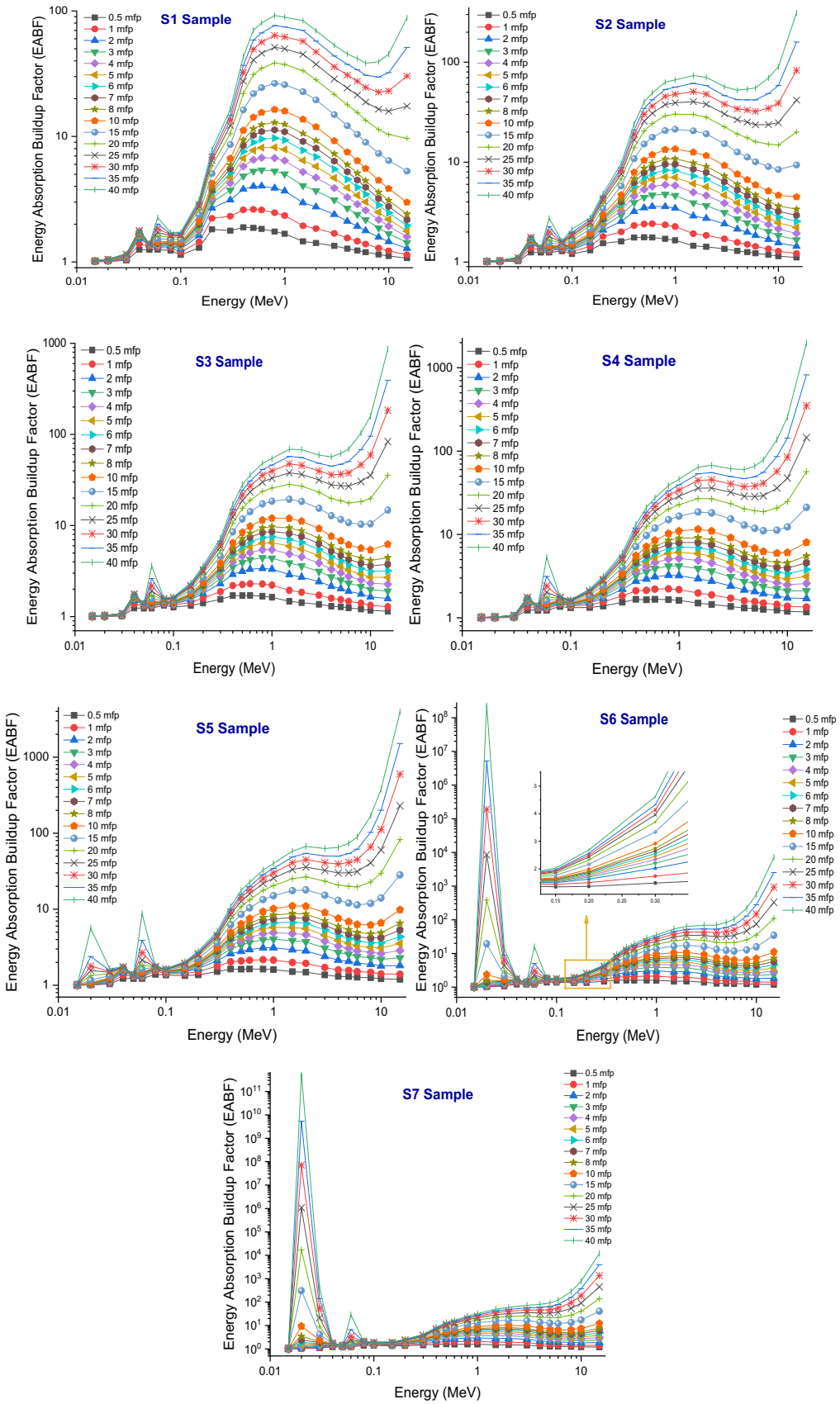

Fig. 10 Variation of EABF values as a function of photon energy at 0.5–40 mfp

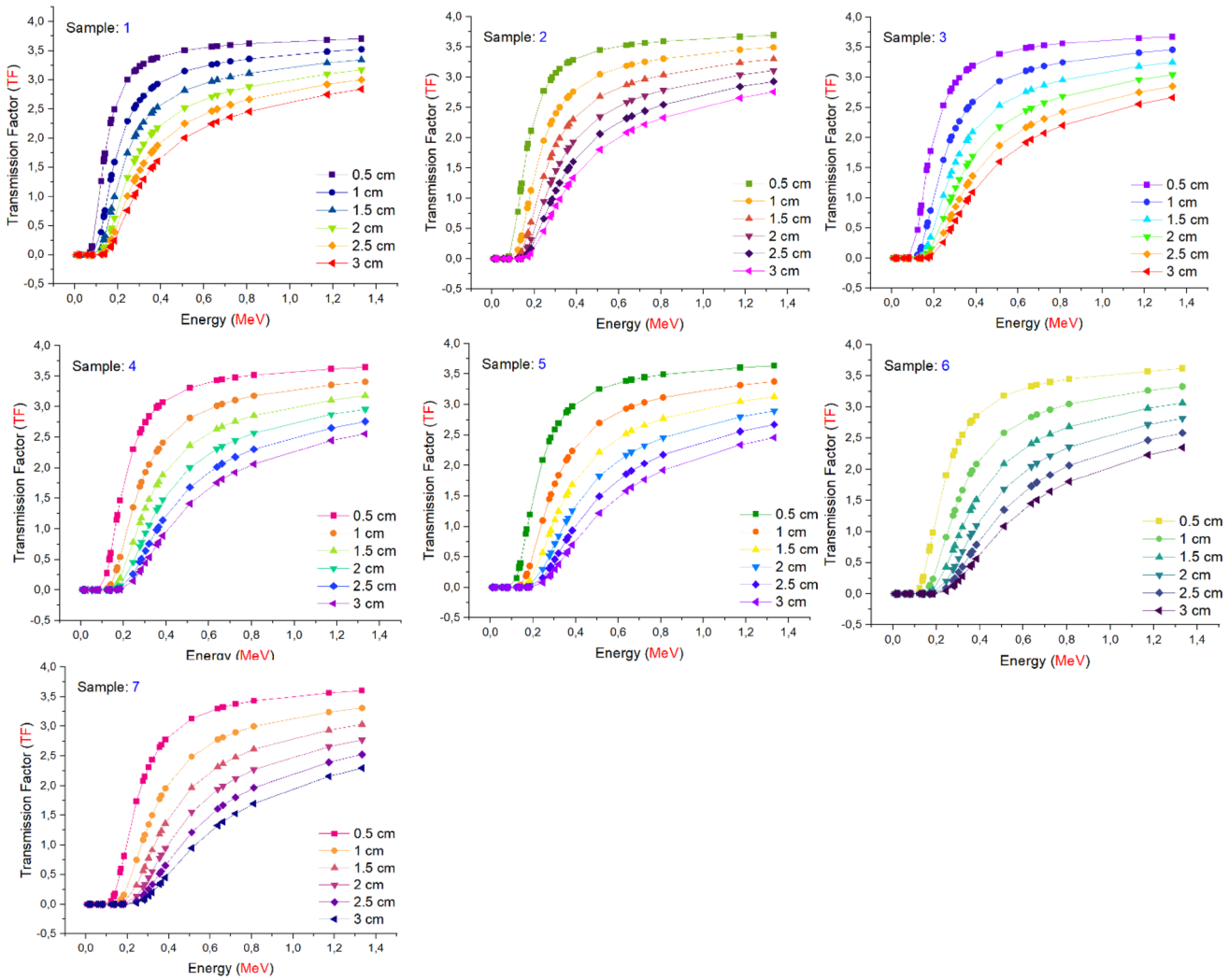

Fig. 11 Transmission factors (TFs) of investigated glasses as a function of used radioisotope energy (MeV) at different glass thicknesses

increases beyond 0.1 MeV, the reactivity of glass samples increases as well. All glass samples were tested at a thickness of 3 cm to find their maximum attenuation (also known as minimum transmission). Increasing shield thickness leads in a decrease in incoming gamma-ray attenuation because shield thickness affects the attenuation capability of any shielding material. Subsequently, the attenuation capabilities of various glass thicknesses (0.5 cm, 1 cm, 1.5 cm, 2 cm, 2.5 cm and 3 cm) were used to assess the TF values of the tested glasses in detail. For example, in Fig. 12, the transmission factors of different glass thicknesses as a function of the radiation energy (MeV) used are shown. This chart shows how TF values drop with increasing gamma-ray energy. A thickness of 3 cm had the lowest TF values of all of the glass samples tested. The S7 sample, on the other hand, showed the least transmission behavior across all the above-mentioned studied glass thicknesses.

4 Conclusion

Recent years have seen a spike in interest in the potential of reinforced glasses for a variety of applications in radiation areas. While this scenario has benefited the development of novel glass combinations and the literature in the material sciences in recent years, it continues to allow for the development of radiation protection settings with the highest possible level of protection. In this study, Phy-X/PSD software and MCNPX Monte Carlo code were applied to investigate the direct effects of tungsten trioxide (WO_3) on gamma radiation attenuation properties of tungsten/barium/phosphate glasses with chemical form $xWO_3–(50\text{-}x/2)BaO–(50\text{-}x/2)P_2O_3$, x = 0 (S1)–60 (S7) in steps of 10 mol%. The increased amount of WO_3 in the glass composition contributed positively to the increase in density and radiation sensing properties. At the lowest and highest WO_3 contributions, a nearly twofold increase

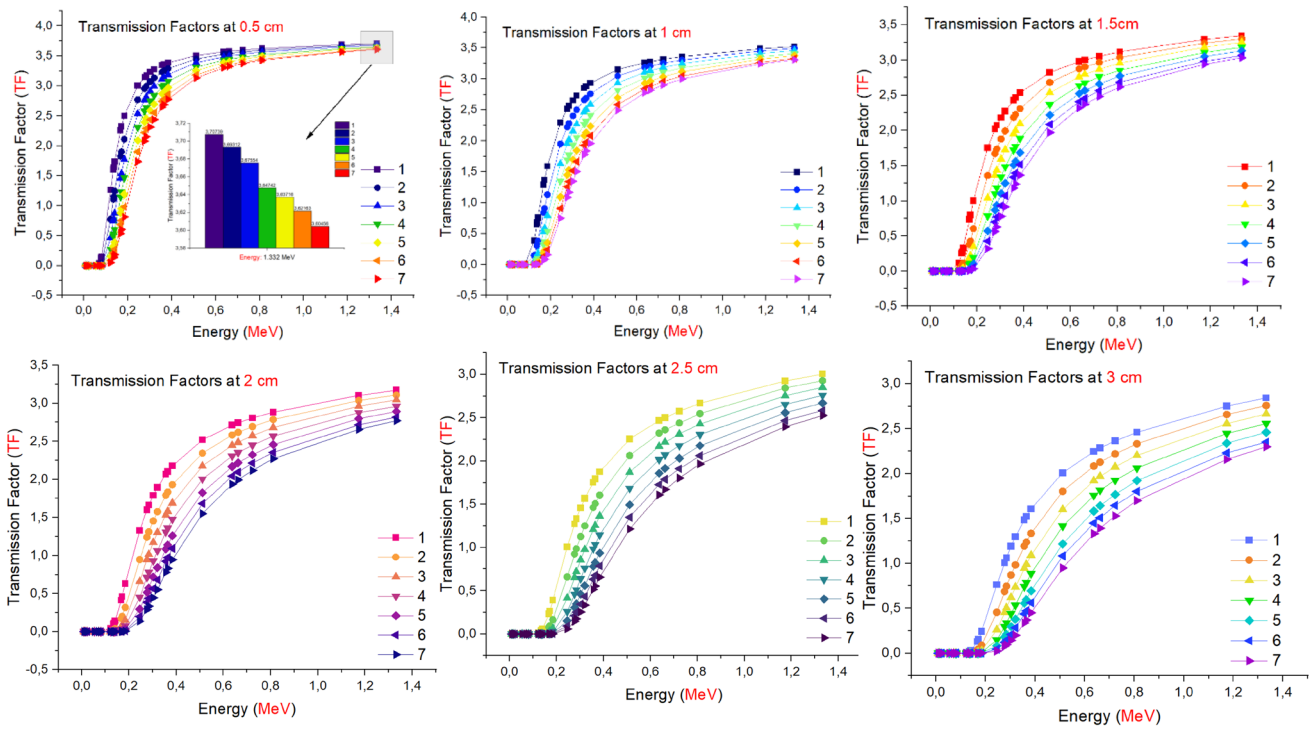

Fig. 12 Comparison of the transmission factors (TFs) as a function of used radioisotope energy (MeV) for different glass thicknesses

in HVL value was seen for the S1 and S7 glass samples, respectively, with S7 having the lowest HVL values. Generally, HVL has followed the trend as: $(HVL)_{S1} > (HVL)_{S2} > (HVL)_{S3} > (HVL)_{S4} > (HVL)_{S5} > (HVL)_{S6} > (HVL)_{S7}$. The variation of the tenth value layer (TVL) for all studied glasses has the same trend of HVL. In terms of mean free path (MFP), there was negative effect of WO_3 concentration on the trend of MFP. Consequently, S7 glass sample has the lowest values of MFP, while the S1 glass sample has the highest values. Therefore, $(MFP)_{S1} > (MFP)_{S2} > (MFP)_{S3} > (MFP)_{S4} > (MFP)_{S5} > (MFP)_{S6} > (MFP)_{S7}$. A comparison of the HVL of S7 glass sample with some commercial radiation shielding materials such as different types of concrete and RS-253-G18 glasses has been performed and concluded that the S7 glass sample is superior as radiation shielding material than several commercial materials. The major purpose of this work was to evaluate the synergistic behavioral changes that occur because of varying degrees of WO_3 heavy metal oxide structure in the glass, as suggested by a review of the literature. Although this research concentrated on glass samples and their elastic, mechanical and gamma-ray-shielding properties as a function of WO_3 content, other factors such as mechanical, thermal, and cost assessments relevant to application settings may be examined in future studies to offer a more complete view of these glass samples for practical applications.

Acknowledgements This work was performed under Princess Nourah Bint Abdulrahman University Researchers Supporting Project Number (PNURSP2022R149), Princess Nourah Bint Abdulrahman University, Riyadh, Saudi Arabia. The authors express their sincere gratitude to Princess Nourah Bint Abdulrahman University.

Funding Princess Nourah Bint Abdulrahman University Researchers Supporting Project Number (PNURSP2022R149).

Data availability The data presented in this study are available on request from the corresponding author.

Declarations

Conflict of interest The authors declare no conflict of interest.

Institutional review board Not applicable.

Informed consent Not applicable.

References

1. N. Singh, K.J. Singh, K. Singh, H. Singh, Comparative study of lead borate and bismuth lead borate glass systems as gamma-radiation shielding materials. Nucl. Instrum. Methods Phys. Res. Sect. B Beam Interact. Mater. Atoms **225**, 305–309 (2004)
2. E. Kavaz, F.I. El Agawany, H.O. Tekin, U. Perişanoğlu, Y.S. Rammah, Nuclear radiation shielding using barium borosilicate glass ceramics. J. Phys. Chem. Solids **142**, 109437 (2020)

3. A. Chahine, M. Et-tabirou, J.L. Pascal, FTIR and Raman spectra of the Na2O–CuO–Bi2O3–P2O5 glasses. Mater. Lett. **58**, 2776–2780 (2004)
4. A. El-Taher, A.M. Ali, Y.B. Saddeek, R. Elsaman, H. Algarni, Kh.S. Shaaban, T. Amer, Gamma ray shielding and structural properties of iron alkali alumino-phosphate glasses modified by PbO. Radiat. Phys. Chem. **165**, 108403 (2019)
5. S.A.M. Issa, M.I. Sayyed, A.M.A. Mostafa, G. Lakshminarayana, I.V. Kityk, Investigation of mechanical and radiation shielding features of heavy metal oxide based phosphate glasses for gamma radiation attenuation applications. J. Mater. Sci. Mater. Electron. **30**, 12140–12151 (2019)
6. E.-S. Waly, G.S. Al-Qous, M.A. Bourham, Shielding properties of glasses with different heavy elements additives for radiation shielding in the energy range 15–300 keV. Radiat. Phys. Chem. **150**, 120–124 (2018)
7. R.G. Jaeger, *Engineering compendiumon radiation shielding, volume II: shielding materials* (Springer-Verlag, International Atomic Energy Agency, Vienna, 1975)
8. N. Singh, K.J. Singh, K. Singh, H. Singh, Gamma-ray attenuation studies of PbO–BaO–B2O3 glass system. Radiat. Meas. **41**, 84–88 (2006)
9. M. Saad, H. Elhouichet, Good optical performances of Eu3+/Dy3+/Ag nanoparticles co-doped phosphate glasses induced by plasmonic effects. J. Alloys Compd. **806**, 1403–1409 (2019)
10. G. Moulika, S. Sailaja, B.N.K. Reddy, V.S. Reddy, S. Dhoble, B.S. Reddy, Optical properties of Eu3+ and Tb3+ ions doped alkali oxide (Li2O/Na2O/K2O) modified boro phosphate glasses for red, green lasers and display device applications. Physica B **535**, 2–7 (2018)
11. M.K. Hwang, I.G. Kim, B.K. Ryu, Study of water resistance of Fe 2 O 3 doped P 2 O 5–ZnO–Bi 2 O 3 sealing glass system, Korean. J Met. Mater. **54**, 621–625 (2016)
12. J. Šantić, L. Nikolić, R.D. Pavić, P. Banhatti, L. Mošner, A. Koudelka, Moguš- Milanković, scaling features of conductivity spectra reveal complexities in ionic, polaronic and mixed ionic-polaronic conduction in phosphate glasses. Acta Mater. **175**, 46–54 (2019)
13. Y.B. Peng, D.E. Day, High thermal expansion phosphate glasses part 2. Glass Technol. **32**, 166 (1991)
14. D.S. Brauer, C. Rüssel, J. Kraft, Solubility of glasses in the system P2O5–CaO–MgO–Na2O–TiO2: experimental and modeling using artificial neural networks. J. Non-Cryst. Solids **353**, 263 (2007)
15. V.P. Singh, N.M. Badiger, N. Chanthima, J. Kaewkhao, Evaluation of gamma-ray exposure buildup factors and neutron shielding for bismuth borosilicate glasses. Radiat. Phys. Chem. **98**, 14–21 (2014)
16. L. Koudelka, J. Šubčík, P. Mošner, I. Gregora, L. Montagne, L. Delevoye, I. Gregora, Glass-forming ability and structure of glasses in ZnO-WO3-P2O5 system. Phys Chem Glasses Eur J Glass Sci Technol B **53**, 79–85 (2012)
17. L. Koudelka, I. Rösslerová, P. Mošner, Z. Černošek, M. Lissová, M. Liška, L. Montagne, L. Delevoye, Structure and properties of lead tungstate-phosphate glasses. Phys. Chem. Glasses Eur. J. Glass Sci. Technol. B **53**, 86–92 (2012)
18. G. Pal Singh, D.P. Singh, Effect of WO3 on structural and optical properties of CeO2–PbO–B2O3 glasses. Phys. B Condens. Matter **406**, 640–644 (2011)
19. Y. Saito, S. Uchida, T. Kubo, H. Segawa, Energy-storable dye-sensitized solar cells with tungsten oxide charge-storage electrode. J. Electrochem. Soc. **16**, 27 (2009)
20. F.G.K. Baucke, K. Bange, T. Gambke, Reflecting electrochromic devices. Displays **9**, 179 (1988)
21. C.G. Granqvist, A. Azens, J. Isidorsson, M. Kharrazi, L. Kullman, T. Lindström, G.A. Niklasson, C.-G. Ribbing, D. Rönnow, M. Strømme Mattsson, M. Veszelei, Towards the smart window: progress in electrochromics. J. Non-Cryst. Solids **218**, 273 (1997)
22. S.A.M. Issa, M. Rashad, A. Hanafy Taha, B. Saddeek Yasser, Experimental investigations on elastic and radiation shielding parameters of WO3-B2O3-TeO2 glasses. J. Non-Cryst. Solids **544**, 120207 (2020)
23. R. El-Mallawany, L. El-Deen, M. Elkholy, Dielectric properties and polarizability of molybdenum tellurite glasses. J. Mater. Sci. **31**, 633943 (1996)
24. H. Qiu, M. Kudo, H. Sakata, Synthesis and electrical properties of Fe2O3-MoO3-TeO2 glasses. Mater. Chem. Phys. **51**, 233e8 (1997)
25. J. Pisarska, R. Lisiecki, W. Ryba-Romanowski, G. Domniak-Dzik, W.A. Pisarski, Up-converted luminescence in YbeTm codoped lead fluoroborate glasses. J. Alloys Compd. **451**, 226e8 (2008)
26. G.P. Singh, P. Kaur, S. Kaur, D.P. Singh, Role of WO3 in structural and optical properties of WO3eAl2O3ePbOeB2O3 glasses. Physica **B406**, 4652e6 (2011)
27. B.H. Jung, D.K. Kim, H.-S. Kim, Properties and structure of (50–x) BaO-xZnO-50P2O5. J. Non-Cryst. Solids **351**, 3356–3360 (2005)
28. A. Saeed, R.M. Elshazly, Y.H. Elbasher, A.M. Abou El-azm, M.M. El-Okr, M.N.H. Comsan, A.M. Osman, A.M. Abdal-monem, A.R. El-Sersy, Gamma ray attenuation in a developed borate glassy system. Radiat. Phys. Chem. **102**, 167–170 (2014)
29. RSICC Computer Code Collection (2002) MCNPX user's manual version 2.4.0. Monte Carlo N-particle transport code system for multiple and high energy applications
30. E. Şakar, Ö.F. Özpolat, B. Alım, M.I. Sayyed, M. Kurudirek, Phy-X/PSD: development of a user friendly online software for calculation of parameters relevant to radiation shielding and dosimetry. Radiat. Phys. Chem. **166**, 108496 (2020). https://doi.org/10.1016/j.radphyschem.2019.108496
31. P. Kalenda, L. Koudelka, P. Mošner, L. Montagne, B. Revel, Glass-forming ability and the structure of glasses in the $BaO-WO_3-P_2O_5$ system. J. Non-Cryst. Solids **541**, 120145 (2020)
32. M.I. Sayyed, B.O. Ashok Kumar, K.A. El-bashir, M.H.M. Mahmoud, H.A.A. Sidek. Zaid, K.A. Matori, Investigation of the mechanical and radiation shielding features for BaO-WO3-P2O5 glass systems. Optik **258**, 168810 (2022). https://doi.org/10.1016/j.ijleo.2022.168810
33. M. Almateri, O. Agar, E.E. Altunsoy, O. Kilicoglu, M.I. Sayyed, H.O. Tekin, Photon and neutron shielding characteristics of samarium doped lead alumino borate glasses containing barium, lithium and zinc oxides determined at medical diagnostic energies. Res. Phys. **12**, 2123–2128 (2019). https://doi.org/10.1016/j.rinp.2019.01.094
34. H.O. Tekin, G. ALMisned, Y.S. Rammah, G. Susoy, F.T. Ali, D.S. Baykal, H.M.H. Zakaly, S.A.M. Issa, A. Ene, Mechanical properties, elastic moduli, transmission factors, and gamma-ray-shielding performances of Bi2O3–P2O5–B2O3–V2O5 quaternary glass system. Open Chem. **20**, 314–329 (2022). https://doi.org/10.1515/chem-2022-0145
35. H.O. Tekin, G. Almisned, G. Susoy, F.T. Ali, D.S. Baykal, A. Ene, S.A.M. Issa, Y.S. Rammah, H.M.H. Zakaly, Transmission factor (TF) behavior of Bi2O3–TeO2–Na2O–TiO2–ZnO glass system: a Monte Carlo simulation study. Sustainability **14**, 2893 (2022). https://doi.org/10.3390/su14052893
36. I.I. Bashter, Calculation of radiation attenuation coefficients for shielding concretes. Ann. Nucl. Energy **24**, 1389–1401 (1997)
37. ⟨http://www.schott.com/advanced_optics/english/products/optical-materials/special-materials/radiation-shielding-glasses/index.html⟩, n.d.